

A SPECTROSCOPIC SEARCH FOR COLLIDING STELLAR WINDS IN O-TYPE CLOSE BINARY SYSTEMS. V. HD 149404

M. L. THALLER¹

Infrared Processing and Analysis Center, California Institute of Technology, MS 100-22, 770 South Wilson Avenue, Pasadena, CA 91125;
thaller@ipac.caltech.edu

D. R. GIES

Center for High Angular Resolution Astronomy, Department of Physics and Astronomy, Georgia State University, Atlanta, GA 30303; gies@chara.gsu.edu

A. W. FULLERTON²

Department of Physics and Astronomy, University of Victoria, P.O. Box 3055, Victoria, BC V8W 3P6, Canada; awf@pha.jhu.edu

L. KAPER

Sterrenkundig Instituut “Anton Pannekoek,” Universiteit van Amsterdam, Kruislaan 403, Amsterdam, SJ NL-1098, Netherlands; lexk@astro.uva.nl

AND

R. WIEMKER

Philips Research Hamburg, Medical Image Analysis, Roentgenstrasse 24-26 D-22335, Hamburg, Germany; Rafael.Wiemker@philips.com

Received 1999 September 3; accepted 2001 January 17

ABSTRACT

We present new H α emission-line spectra and an analysis of the mass outflow for the massive close binary HD 149404. Spectra obtained between 1995 and 1997 show evidence of coherent orbital phase-related variations superimposed on both long-term and short-term emission strength variations. We use a Doppler tomography algorithm to construct velocity maps of the emission intensity, and these demonstrate that emission displays two broad peaks that follow sinusoidal radial velocity curves that are significantly different from the orbital velocity curves of either star. We present a model for the kinematics and distribution of the emitting circumstellar gas, and we argue that most of the emission comes from wind flows from both stars into a shock region between them. The binary appears to be in a post-mass transfer stage in which systemic mass loss dominates the evolutionary processes.

Subject headings: binaries: close — binaries: spectroscopic — line: profiles — stars: early-type — stars: individual (HD 149404) — stars: mass loss

1. INTRODUCTION

Radiatively driven winds are found in all massive luminous stars, and in close binary systems the individual winds may collide and form a bow shock that wraps around the star with the weaker wind. One easily observable consequence of colliding winds is H α emission. This emission is an excellent probe of dense regions in the wind, since it is caused by recombination, in which the emissivity scales with the square of the density. Enhanced density is expected in two places, the lower layers of the wind near the photosphere of the generating star and near the shock. The lower wind contribution to H α comes from layers typically between 1.0 and 1.5 stellar radii (Puls et al. 1996). Such base-level emission will show radial velocity variations similar to the stars themselves. Emission formed in the shock region, on the other hand, will display velocity variations defined by the spatial and velocity structure of the circumstellar gas. These velocity curves are often quite different from the motion of the stars. Several groups have made H α studies of massive binary systems and deduced the presence of colliding winds (Vreux 1985; Gies & Wiggs 1991; Wiggs & Gies 1992, 1993; Gies, Wiggs, & Bagnuolo 1993).

Thaller (1997) undertook an all-sky H α survey of massive binaries to search for likely colliding winds candidate

systems. She identified HD 149404, composed of a supergiant and a giant star, as an especially promising system for the detection of wind-induced shocks. HD 149404, composed of a supergiant and giant star, is one of the brightest members of the Ara OB1 association. H α emission was first observed by Kucewicz (1963), and a double-peaked structure to the emission was observed by Jaschek, Jaschek, & Kucewicz (1964), suggesting that HD 149404 is a binary. Supporting this notion, Hutchings (1976) found HD 149404 to be a radial velocity variable. Conti, Leep, & Lorre (1977) discovered a double-lined spectrum for the system, and the first orbital elements were determined by Massey & Conti (1979), who set the period at 9.813 days. Massey & Conti hypothesized that the H α emission seen in this system could be indicative of current large mass loss. They determined that the brighter star (estimated to be an O8.5 I) was less massive than the dimmer, hotter star [O7 III(f)], which also suggested a history of mass loss or mass transfer. Stickland & Koch (1996) used cross-correlation techniques with UV spectra from the *International Ultraviolet Explorer* satellite and found a similar period of 9.8145 days, again with the dimmer star as the more massive component ($M_2/M_1 = 1.53 \pm 0.09$). In addition, Stickland & Koch (1996) noticed a strengthening of the lines of the dimmer star during its quadrature of greatest blueshift, a classic “Struve-Sahade effect” (Gies, Bagnuolo, & Penny 1997). HD 149404 is also a known *IRAS* infrared source and a radio emitter at 3.6 cm (Lamers & Leitherer 1993), further indications of extensive mass loss and the likely presence of circumstellar material in the system. This system presents an interesting problem to stellar nomenclature. The brighter star was originally iden-

¹ Visiting Astronomer, Mount Stromlo and Siding Springs Observatories, Australian National University.

² Postal Address: FUSE Science Center, Department of Physics and Astronomy, Johns Hopkins University, 3400 North Charles Street, Baltimore, MD 21218.

tified as the “primary” star, while in fact, the dimmer star is the more massive (and hotter) of the two. In order to avoid confusion in this paper, the bright supergiant star will be referred to as “Star 1” and the dimmer, more massive giant star, “Star 2.” Note that the system has no known close visual companion (Mason et al. 1998), so we can assume that the spectral features form only in these two stars and their immediate vicinity.

The basic properties of HD 149404, as well as its exact evolutionary status, are subject to considerable debate. Using a tomography technique to separate the individual spectra (Bagnuolo, Gies, & Wiggs 1992), Penny (1996) obtained spectral types of O8.5 I and O6.5 III using UV classification criteria. Penny then used the single star evolutionary tracks of Schaller et al. (1992) to estimate the masses of the stars, $M_1 = 44 \pm 5$ and $M_2 = 49 \pm 12 M_\odot$, respectfully, and their ages, $\approx 3 \times 10^6$ yr. Using her estimate of the inclination ($i = 21^\circ$), Penny determined that both stars in HD 149404 were rapid rotators, with nearly twice the synchronous rotation rate. While the advanced evolutionary state and low mass of Star 1 suggest that mass transfer has occurred in the past, the huge rotational velocities seem inconsistent with the dynamics of Roche lobe overflow, which should force synchronous rotation.

Hoping to resolve some of these inconsistencies, Penny, Gies, & Bagnuolo (1999) analyzed a light curve of HD 149404 from the *Hipparcos* satellite (Perryman 1997). Although the variations in intensity are small (approximately 0.04 mag), the light curve shows a clear ellipsoidal variation. No eclipses were observed, however, which placed a tighter constraint on the inclination of the system. Penny’s new estimate ($i = 30^\circ$) brought the stars’ equatorial velocities down ($V_{\text{eq}1} = 172$ and $V_{\text{eq}2} = 109$ km s $^{-1}$) but still showed them to be rotating faster than synchronous. A major change, however, occurred in Penny’s estimate of the stellar masses. With the new inclination, she estimated the masses to be 16 and 18 M_\odot for Stars 1 and 2, respectively. In addition, the new parameters suggest that Star 1 is very close to filling its Roche lobe.

Penny et al. (1999) proposed that HD 149404 has experienced mass loss (or possibly mass transfer) in the past, which has now ceased. They suggest that Star 1, originally the more massive, lost mass through Roche lobe overflow, which may or may not have accreted onto the other star. This mass loss increased the mass ratio above unity, making Star 2 more massive, and led to greater separation of the stars. The current supersynchronous rotation rates may reflect the synchronous rotation of an earlier, shorter period system. The rotational velocities may partially account for the surprisingly low masses of the stars, since rapidly rotating stars have larger mass-loss rates than those found in nonrotating stars (Maeder 1999). Penny’s scenario agrees well with suggestions by Vanbeveren & de Loore (1980) and Hutchings & Van Heteren (1981) that Star 1 is a post-Roche lobe overflow object. The apparent lack of C III and extreme strength of the N III lines found by Jaschek & Jaschek (1974) also suggest past mass loss by Star 1, which has resulted in the exposure of nuclear processed materials at the surface of the star. In the UV region of the spectrum, however, Penny (1996) found normal carbon line strengths for the supergiant star, so the situation may not be that simple.

In this paper, we report on a detailed study of the orbital phase-related variations of the H α line. We show that

coherent emission variations are present, but they have radial velocity patterns that differ from the orbital motion of either star. We present an analysis of these motions, aimed at determining the location of the emitting gas in the system. This analysis suggests that the emission originates in the gas flows from each star toward a central colliding winds zone and that we are witnessing an evolutionary stage in which wind mass loss dominates over binary mass transfer.

2. OBSERVATIONS AND REDUCTIONS

Two independent groups, one at Georgia State University (GSU) and one at the European Southern Observatory (ESO), obtained H α spectra of HD 149404. The GSU observations were obtained with the 74 inch telescope at the Mount Stromlo Observatory (MSO) on the nights of 1996 March 3–12, using the coudé spectrograph, grating C (600 grooves mm $^{-1}$, blazed at 12,500 Å in first order) in second order, and the 81.3 cm focal length camera. This produced a spectral coverage of 6648–6740 Å with a reciprocal dispersion of 0.24 Å pixel $^{-1}$ on a thinned 2048 × 2048 Tektronix CCD detector (Tek 2K). An RG610 filter was used to block higher orders. The exposure times ranged from 5 to 20 minutes depending on sky conditions, and several bias, flat-field, and Th-Ar comparison lamp spectra were obtained each night. In addition, several spectra of the rapidly rotating star HD 87901 were taken each night to facilitate later telluric line removal. A second run on the Mount Stromlo 74 inch telescope took place on the nights of 1997 March 20–April 1. The arrangement was identical to the first Mount Stromlo run, with the exception of the detector, which was a 4096 × 2048 SITE CCD. This produced a wavelength coverage of 6342–6962 Å and a reciprocal dispersion of 0.152 Å pixel $^{-1}$. For both observing runs, we were able to obtain data with a signal-to-noise ratio of 200–300 pixel $^{-1}$ in the continuum.

The MSO data were extracted and calibrated using standard routines in IRAF.³ Subsequently, the spectra were rectified to a unit continuum using a cubic spline fitted to line-free regions. The spectra were then cross-correlated with a library of purely telluric spectra obtained from images of the rapidly rotating standard star. Each target spectrum was divided by the best-fit telluric spectrum, leaving the resulting spectrum free of atmospheric lines. Next, the spectra were cleaned of remaining cosmetic imperfections by interpolation. Finally, spectra from each run were interpolated onto a common heliocentric wavelength grid.

We also obtained H α spectra of HD 149404 at ESO with the coudé auxiliary telescope (CAT) and coudé echelle spectrometer on the nights of 1995 May 29–June 6, using the red-optimized path with CCD 34 (2048 × 2048 pixels), windowed to 40 pixels in the cross-dispersion direction, as a detector. This arrangement produced a spectral coverage of 6533–6594 Å with a reciprocal dispersion of 0.029 Å pixel $^{-1}$ and a typical signal-to-noise ratio of 250 pixel $^{-1}$. The spectra were wavelength calibrated using Th-Ar spectra obtained every 2 hr. These spectra were extracted, calibrated, and telluric cleaned using the MIDAS software

³ IRAF is distributed by the National Optical Astronomy Observatories, which is operated by the Association of Universities for Research in Astronomy, Inc., under cooperative agreement with the National Science Foundation.

package. Note that the wavelength coverage of the ESO CAT spectra is relatively small (about 50 Å) so that the rectification of the profile to a unit continuum may be based on the extreme wings of the emission profile rather than the true stellar continuum (see below).

3. VARIATIONS IN H α EMISSION

We begin by considering the orbital phase–related variations in the spectra. We calculated orbital phases using the ephemeris of Stickland & Koch (1996): $P = 9.81452$ days and $T_0 = \text{HJD } 2,444,449.303$, where zero phase corresponds to the maximum radial velocity of Star 1 in this circular orbit. A journal of observational dates and phases is given in Table 1. Figure 1 shows the ESO H α spectra plotted as a function of orbital phase and radial velocity, assuming a rest wavelength of 6562.682 Å, while Figure 2 shows the same for the two MSO runs. The spectra are placed in the diagram so that their continua are aligned with the orbital phase of observation. The bar in the upper right-hand corner indicates the intensity scale relative to the continuum. The H α line shape shows a clear progression with orbital phase, changing from single- to double-peaked twice during the orbit. However, the patterns are not those expected from the orbital motion of the stars (see below).

Inspection of Figures 1 and 2 shows that there are also significant variations in H α strength that are unrelated to orbital phase. The profile apparently changed in overall strength between 1995 and 1996–1997. Equivalent widths

(from numerical integration and with errors of $\approx 10\%$) are listed in Table 1 and plotted versus orbital phase in Figure 3. The emission strength appears to have increased from $W_\lambda = -4.6$ Å in 1995 to $W_\lambda = -6.5$ Å in 1996 and 1997. This may be due in part to our rectification scheme that involved fitting the extreme line wings in the ESO spectra (see above), which might lead to systematically lower equivalent widths. On the other hand, we doubt the difference is caused by differences in scattered light properties of the two spectrographs because observations of other binaries from ESO and MSO do not show this discrepancy. However, changes of this magnitude are seen in the H α emission of some single O supergiants (Kaper et al. 1998). The detailed profile shape also shows evidence of long-term changes (see, for example, the extended blue wing found in the MSO 1996 spectra in the phase range 0.0–0.3). Furthermore, there are variations on timescales of days superimposed on the orbital phase–related variations (see the large differences near line center at phase 0.4 between spectra obtained within the 1996 and 1997 runs). Thus, although we will focus attention on the orbital shape variations in the discussion below, the variations in equivalent width on other timescales clearly indicate that the outflows that produce the H α emission are transitory in nature. Given these substantial variations, there is no compelling evidence that the emission equivalent width is phase dependent.

The lack of substantial equivalent width variations related to the orbital cycle suggests that no significant occultation of the emitting regions by the stars occurs during the orbit. This is not surprising given the system's low orbital inclination ($i = 30^\circ \pm 5^\circ$; Penny et al. 1999). The orbital phase variations in the shape of H α appear to result from the changing viewing angle with orbital phase of a mainly optically thin emitting gas that has an anisotropic velocity distribution. Because the orbit is essentially circular (Stickland & Koch 1996), we expect that each element of gas in the volume will appear to show orbital phase–related Doppler shifts dependent on the motion of that element. It is also reasonable to assume that gas motions are symmetric with respect to the orbital plane.

These conditions are ideal for the application of a Doppler tomography algorithm to reconstruct the velocity distribution of the emitting gas using the ensemble of emission-line profiles from around the orbit. Doppler tomography is now an important tool in emission-line studies of cataclysmic variables (Kaitchuck et al. 1994) and Algol binaries (Richards, Jones, & Swain 1996), and it has a direct application in the current study. The algorithm seeks to find an emission intensity distribution in a velocity grid plane, (V_x, V_y) (where X is defined by the axis joining the stars), such that the integrated emission as seen from various view angles (or back projections) matches the observed, one-dimensional emission profile. There are many approaches in medical imaging to solving this problem, and astronomers have generally embraced Fourier techniques that work well if the observations have good phase coverage (Kaitchuck et al. 1994). Our data sets have, unfortunately, some significant phase gaps, and so we have used instead an iterative least-squares technique that starts with an empty field and slowly builds up the emission distribution through corrections derived from the ensemble of observed emission profiles. This approach is a direct extension to an $N \times N$ reconstruction of the methods we have applied to the $N \times 2$ reconstructions used to separate the spectra of binary stars

TABLE 1
OBSERVATIONS OF HD 149404

HJD	Orbital Phase	W_λ (Å)	Observatory/Year
2,449,867.5899	0.0685	−4.89	ESO 1995
2,449,867.8031	0.0901	−4.87	ESO 1995
2,449,868.5400	0.1653	−4.51	ESO 1995
2,449,868.6741	0.1790	−4.77	ESO 1995
2,449,868.8327	0.1951	−4.59	ESO 1995
2,449,869.5451	0.2677	−4.81	ESO 1995
2,449,869.6552	0.2789	−4.88	ESO 1995
2,449,869.7825	0.2919	−4.71	ESO 1995
2,449,870.5891	0.3740	−4.28	ESO 1995
2,449,870.7447	0.3899	−4.22	ESO 1995
2,449,871.6361	0.4807	−4.41	ESO 1995
2,449,871.8134	0.4988	−4.29	ESO 1995
2,449,872.5903	0.5779	−4.35	ESO 1995
2,449,872.7294	0.5921	−4.42	ESO 1995
2,449,872.8544	0.6049	−4.48	ESO 1995
2,449,873.5600	0.6768	−4.58	ESO 1995
2,449,873.7567	0.6968	−4.53	ESO 1995
2,449,874.6598	0.7888	−4.65	ESO 1995
2,449,874.8359	0.8068	−4.51	ESO 1995
2,450,148.2334	0.6632	−5.53	MSO 1996
2,450,152.1624	0.0635	−6.54	MSO 1996
2,450,153.1770	0.1669	−7.25	MSO 1996
2,450,154.1908	0.2702	−7.02	MSO 1996
2,450,155.1266	0.3655	−6.00	MSO 1996
2,450,155.1385	0.3667	−6.45	MSO 1996
2,450,528.1580	0.3737	−5.53	MSO 1997
2,450,530.0721	0.5687	−6.55	MSO 1997
2,450,531.0629	0.6696	−7.22	MSO 1997
2,450,534.0516	0.9741	−7.02	MSO 1997
2,450,535.0399	0.0748	−5.99	MSO 1997
2,450,536.0366	0.1764	−6.46	MSO 1997
2,450,538.0418	0.3807	−6.50	MSO 1997

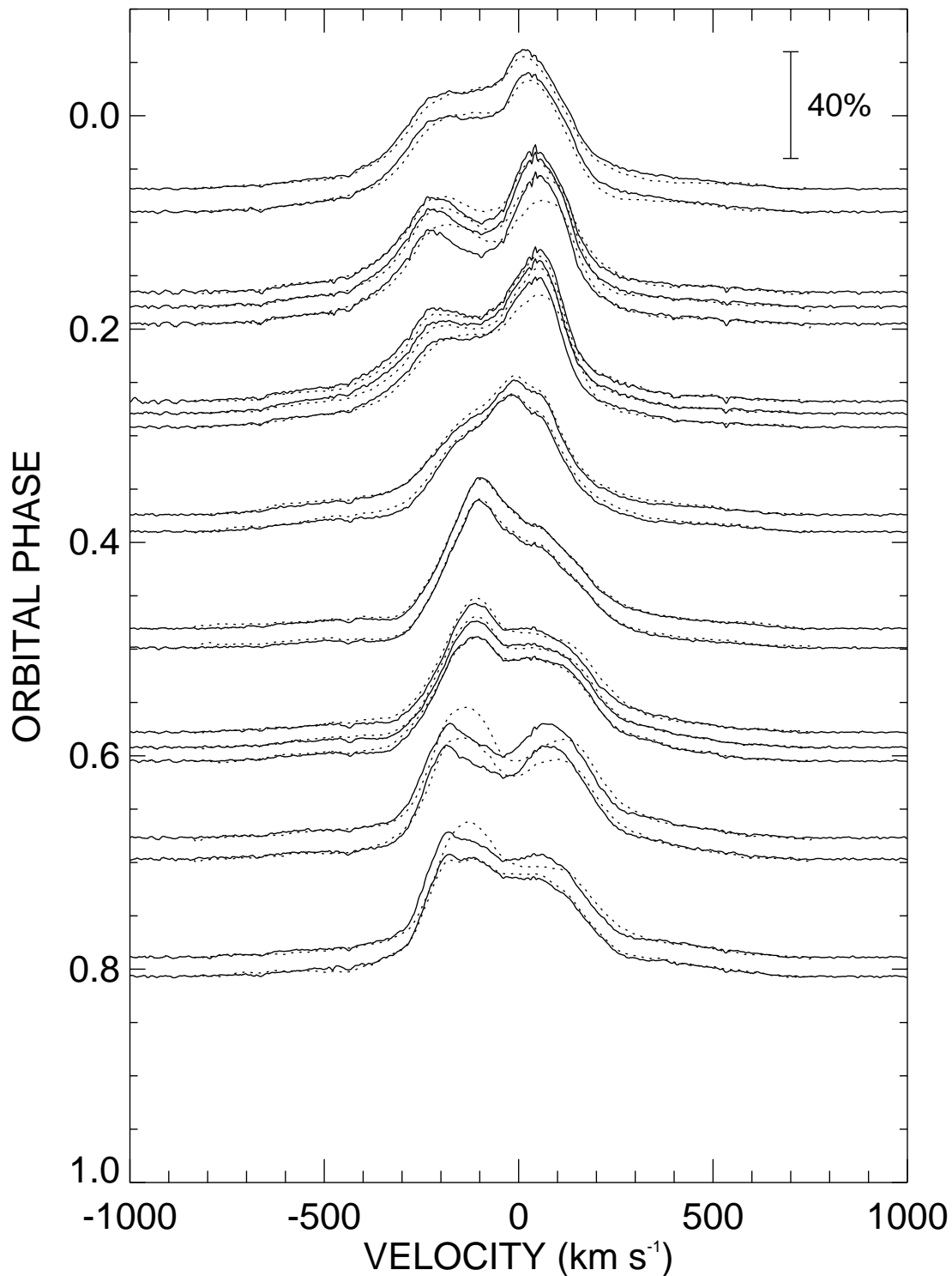


FIG. 1.—H α line profiles obtained at ESO in 1995 plotted against heliocentric radial velocity and arranged in order of orbital phase (phase 0 corresponds to Star 1 maximum radial velocity). Solid lines represent the observations, while dotted lines show model profiles reconstructed from the tomogram.

(Bagnuolo et al. 1992). The code was written in interactive data language (IDL)⁴ by R. Wiemker.

We chose to apply the tomography algorithm separately to the ESO and MSO data sets because of the overall change in emission strength observed between these epochs of observation. The first task in this application is to reset

the continuum to a zero value and then create a velocity grid corresponding to the “center of motion” of the emission. Ideally, this adopted central velocity would be equal to the systemic velocity of the binary. However, there is considerable uncertainty about the actual systemic velocity of HD 149404 because the spectral features measured for radial velocity participate in the photospheric expansion and wind outflow, and the resulting values cover the range

⁴ IDL is a registered trademark of Research Systems, Inc.

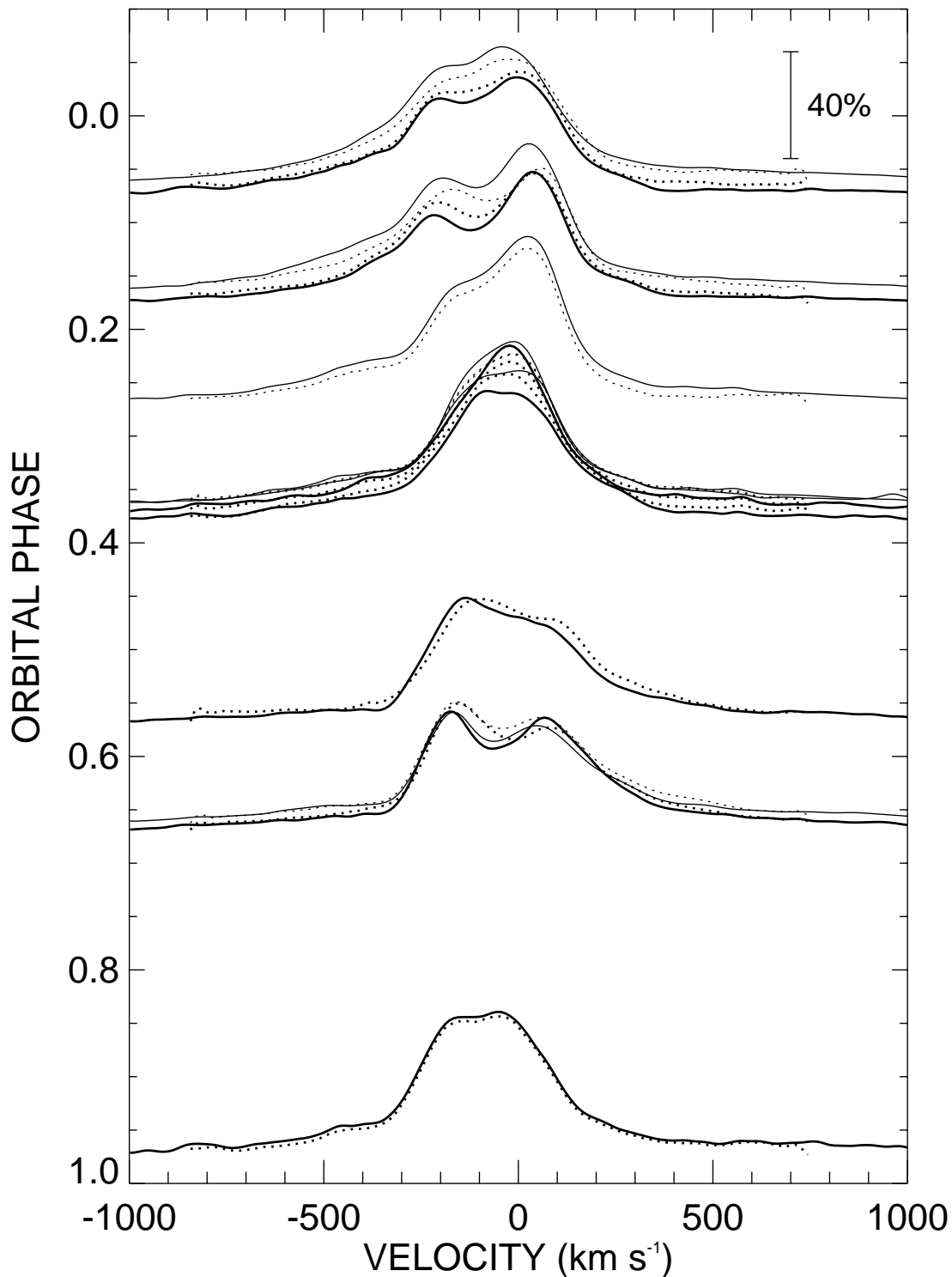


FIG. 2.—H α line profiles obtained at MSO in 1996 (*thin lines*) and in 1997 (*thick lines*) plotted against heliocentric radial velocity and arranged in order of orbital phase. Solid lines represent the observations, while dotted lines show model profiles reconstructed from the tomogram.

from $V_0 = -28$ to -60 km s^{-1} (Massey & Conti 1979; Penny 1996; Stickland & Koch 1996). We decided to find the central velocity from the profiles themselves by forming a global average of all the profiles from a run and then calculating the first moment of the average (equal to -40.3 km s^{-1} for the ESO set and -47.5 km s^{-1} for the MSO sets). We then ran the tomography algorithm for a projected velocity grid from -800 to $+800$ km s^{-1} ; this amounted

to a 233×233 (144×144) velocity grid image for the ESO (MSO) data. We took the viewing angles directly from the orbital phases listed in Table 1, and we ran the tomography procedure for 100 iterations with a gain of 0.8 (the results are insensitive to the values of either parameter).

The resulting tomograms are illustrated as gray-scale images in Figures 4 and 5 for the ESO and MSO data sets, respectively. The gray-scale intensity is shown as a fraction

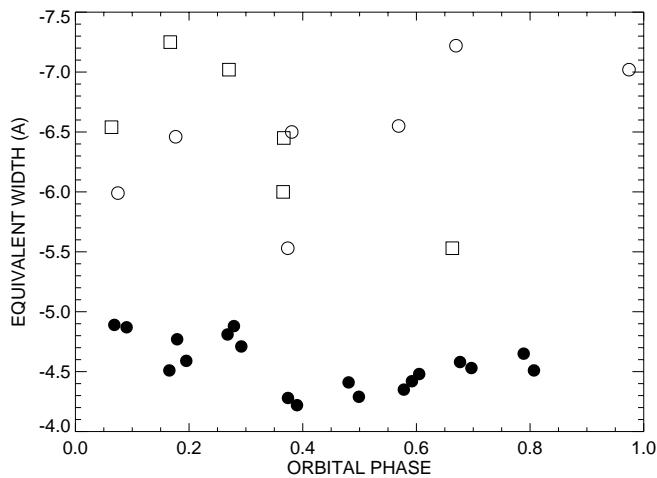


FIG. 3.— $H\alpha$ equivalent width measurements as a function of orbital phase. Filled circles represent ESO observations, while open squares and circles represent MSO observations from 1996 and 1997, respectively.

of the peak intensity in the tomogram (with identifying contour levels given), and for the purposes of illustration, the image was rescaled omitting the lower 20% of emission intensity (which is partially marred by low-level artifacts of the reconstruction). The observed emission profile at any given orbital phase is given by a projection through the image at a particular angle. For example, the projection for phase 0.25 corresponds to the integration of emission intensity along rays from the top to the bottom of the figure. The tomogram predicts that we observe at that phase a broad, double-peaked feature that is more intense at positive velocities, just as observed at this phase (Fig. 1). In fact, we made projections through the tomograms at the observed phases in order to directly compare the expectations from the reconstruction with the actual observations. These model back-projected profiles are shown as dashed lines in Figures 1 and 2, and they generally make a satisfactory match of the observations. This result gives us confidence that the tomograms are indeed an adequate representation of the $H\alpha$ emission velocity distributions as projected on the orbital plane.

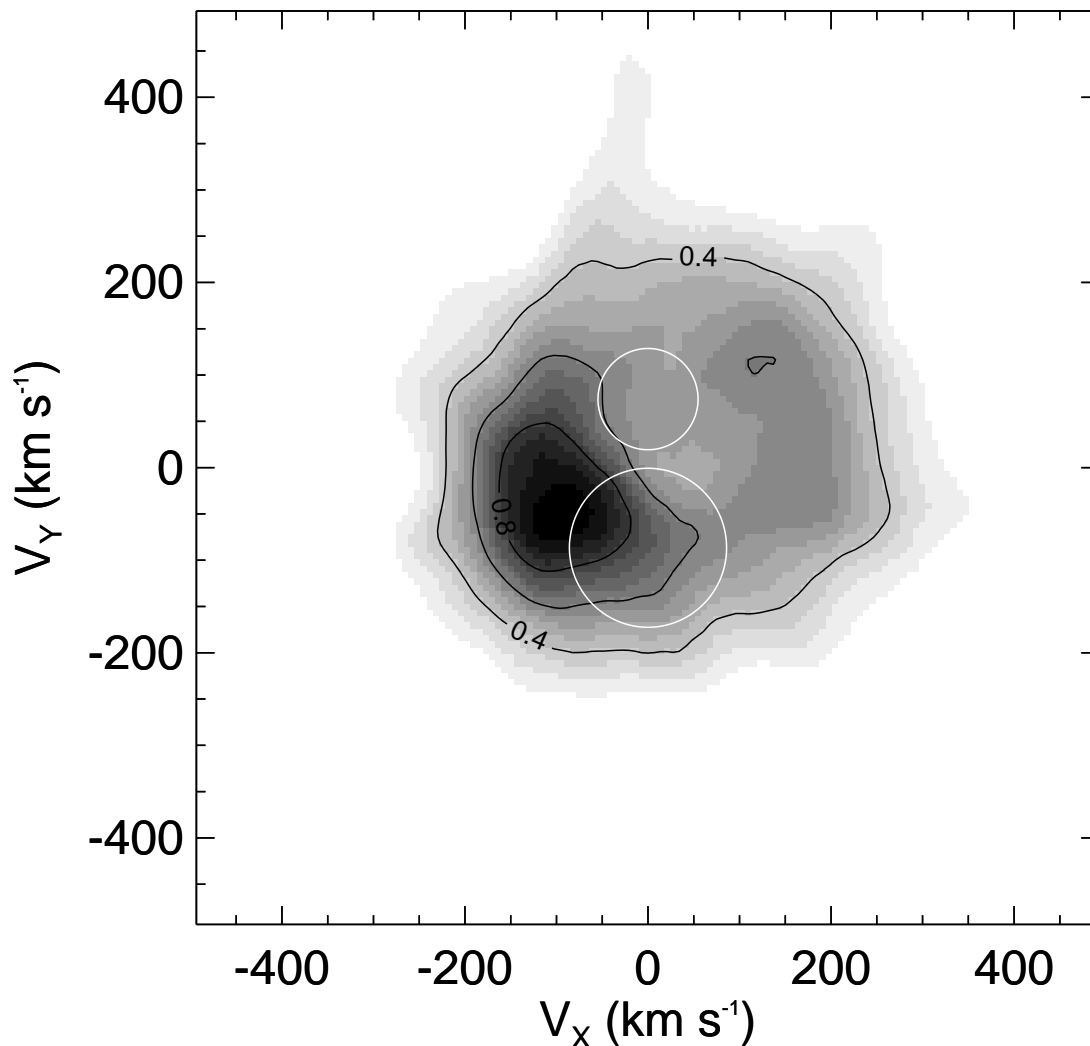


FIG. 4.—Tomogram representation of the $H\alpha$ emission from ESO observations. The gray-scale image gives the emission intensity (as a fraction of the peak value) for the velocity distribution seen in projection at different orbital phases. The variable V_x refers to motion along the axis joining the stars, while V_y is perpendicular to this axis. Observations at orbital phases 0.0, 0.25, 0.5, and 0.75 correspond to projections of this image as seen from the left-hand side, above, right-hand side, and below, respectively. The open circles in white represent the $V \sin i$ limits of Star 1 (*below*) and Star 2 (*above*).

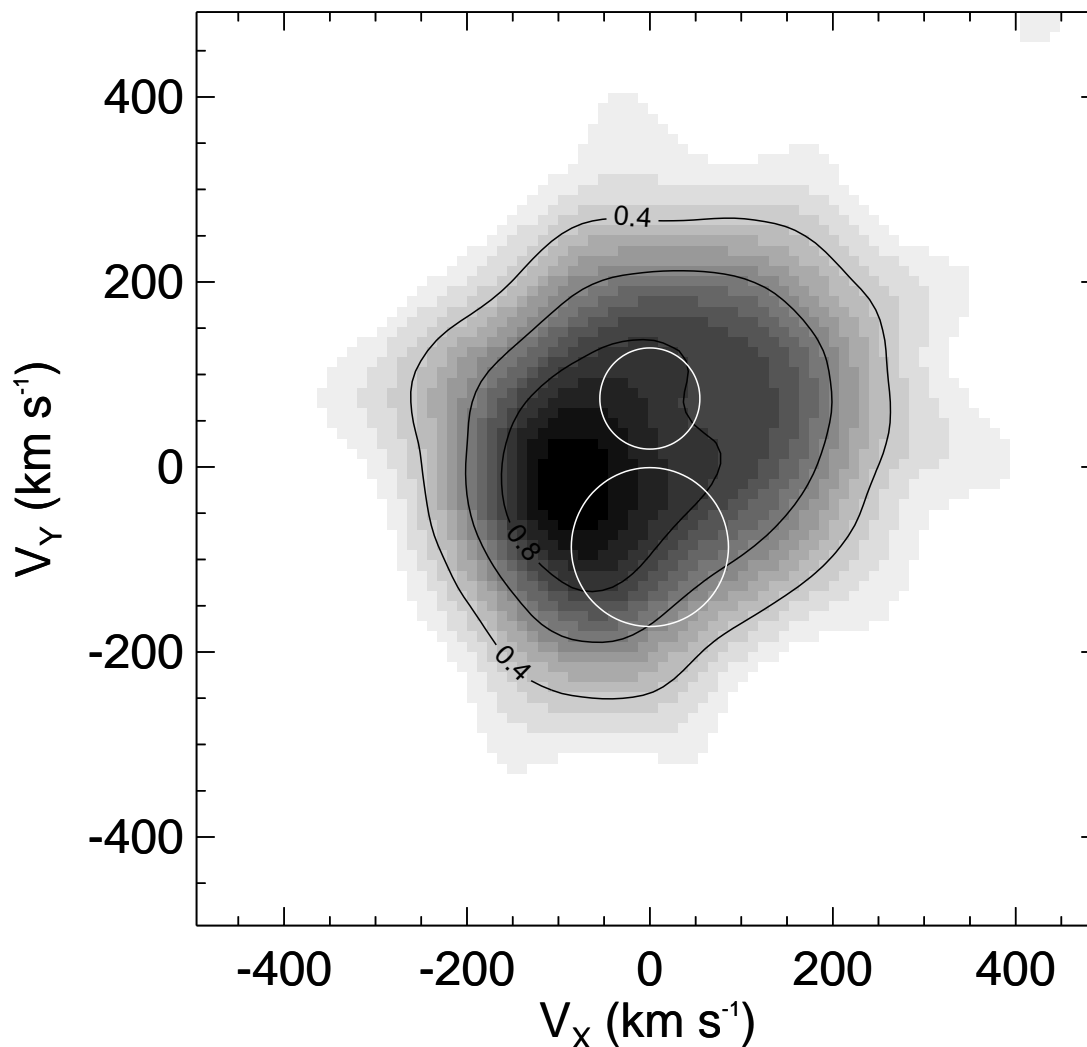


FIG. 5.—Tomogram representation of the H α emission from MSO observations in the same format as Fig. 4

Figures 4 and 5 also show white circles, which indicate the projected rotational velocity limits of the two stars in this velocity grid. The center of Star 1 (*lower circle*), for example, attains greatest positive radial velocity at phase 0.0 (our phase definition), and at that phase the projections of the two rotational velocity broadening distributions are barely resolved. We see that the emission has a fundamentally different velocity distribution from that of the two stars and, in fact, shows motions orthogonal to those of the stars. The emission distribution is centered more or less on the center of mass of the system, and both data sets show subsidiary peaks that are distributed along the V_x axis. There are two peaks in the ESO tomogram, a strong one centered near $V_x = -96$ and $V_y = -48$ km s $^{-1}$ and a weaker peak near $V_x = +116$ and $V_y = +110$ km s $^{-1}$. These two peaks correspond to the two components that appear to separate and merge in the observed profiles (Fig. 1). The MSO tomogram shows similar properties, with a strong peak near $V_x = -85$ and $V_y = -19$ km s $^{-1}$ and an asymmetric extension into the upper right-hand quadrant that corresponds to the weaker peak seen in the ESO tomogram. The differences are partially attributable to the lower resolution of the MSO spectra, but they may also reflect real differences in the emission distribution between these epochs. In the next section, we explore how these tomograms can be

interpreted in terms of gas flows into a colliding winds bow shock.

4. A COLLIDING WINDS MODEL FOR HD 149404

Both stars in this system are expected to have significant stellar wind outflows based on their spectral classifications, and the presence of winds is evident in the strong UV P Cygni lines (Hutchings & Van Heteren 1981) and radio emission (Lamers & Leitherer 1993). Here we explore a wind outflow geometry that could potentially explain the orbital variations in the H α emission. We present in Figure 6 a schematic drawing of HD 149404 as viewed from above the orbital plane, with dimensions from Penny et al. (1999). This view is probably very close to the way the binary actually appears in the sky, due to the low inclination ($i = 30^\circ$) of the system. Based on the observed ellipsoidal variation, Penny et al. find that Star 1 is close to filling its critical Roche surface, and the diagram uses their estimates of volume equivalent radii, $R_1/R_\odot = 23$, $R_2/R_\odot = 16$; semi-major axis, $a/R_\odot = 62$; and mass ratio, $M_2/M_1 = 1.17$. The center of mass (*solid dot*) would be shifted toward Star 2 (from the illustrated position at $x/a = 0.54$ to 0.60) if the mass ratio from Stickland & Koch (1996) is adopted. The luminosities of the stars are almost identical according to Penny et al. (since Star 2 is hotter and smaller), and both

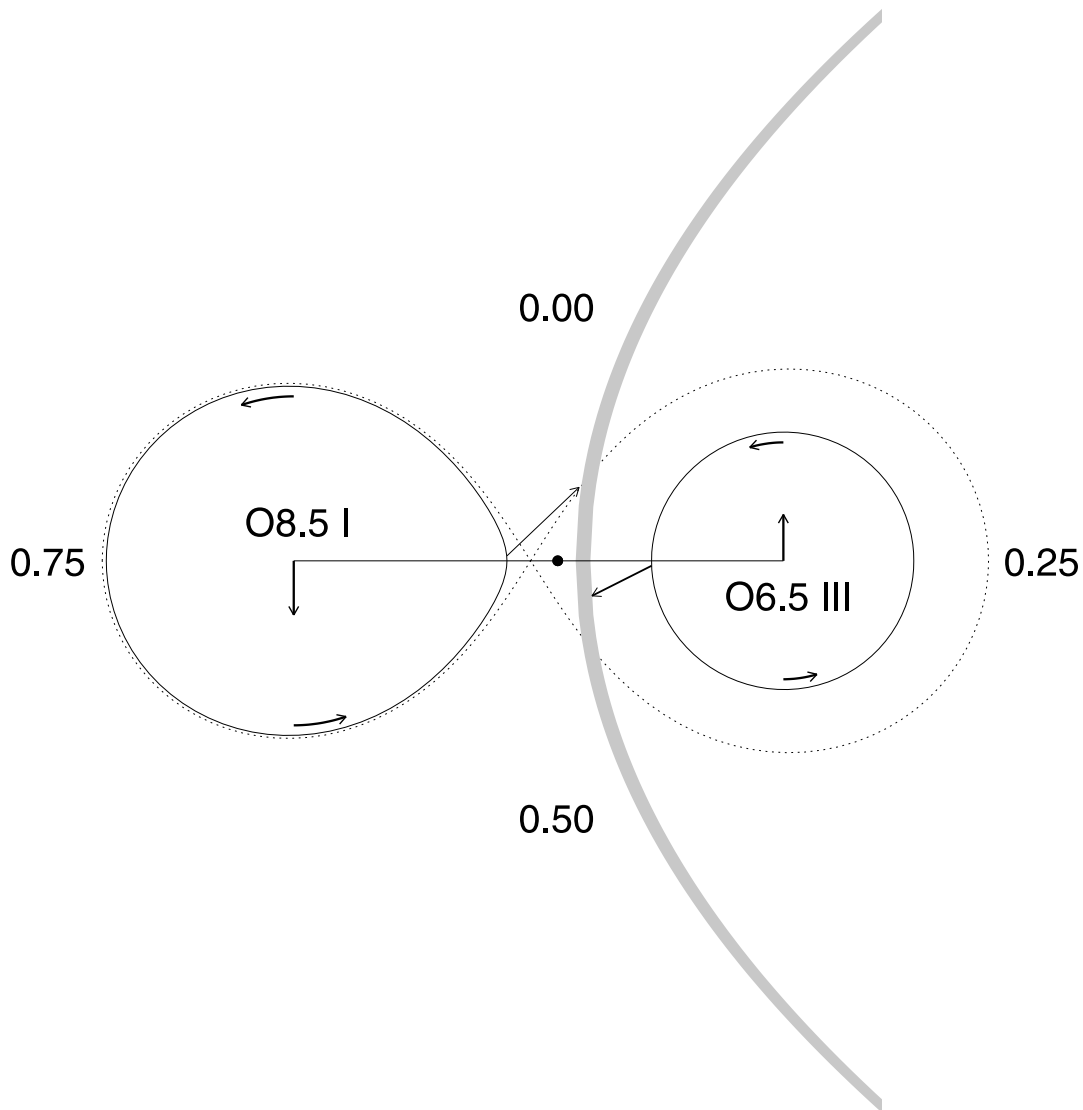


FIG. 6.—View of HD 149404 as seen from above the orbital plane. The dotted line indicates the classical Roche surfaces. The solid dark curves outline the presumed photospheres of the stars. Curved arrows inside the stars represent their equatorial rotational velocities. The center of mass is indicated by a solid dot on the axis joining the two stars, and orbital phases are shown on the periphery in the direction of the observer. The shaded area indicates the likely location of the colliding winds shock. The arrows between the stars show the velocity vectors of the H α emission peaks (heavy line for the strong component and thin line for the weak) for the proposed gas flow configuration.

should have comparable mass-loss rates because of their radiatively driven winds. Penny et al. note that both stars are rotating faster than synchronously ($\Omega/\Omega_{\text{syn}} = 1.4$ and 1.3 for Stars 1 and 2, respectively).

The tomograms provide several hints about the site of the H α emission. The emission velocity distributions illustrated in Figures 4 and 5 are both centered on velocity coordinates associated with the system center of mass and show little or no evidence of orbital motion (which would displace the emission distribution along the V_Y -axis where the stars' orbital velocity components are situated). This central distribution implies that the emitting gas cloud is also centered on the system center of mass, which is found in the gap between the stars (Fig. 6).

A second clue about the placement of the emission comes from inspection of the differences between the observed and reconstructed profiles in Figures 1 and 2. We see that the tomographic reconstructions are generally a good match *except* at the conjunction phases (0.25 and 0.75). At both

conjunctions, we find that the red, receding peak is stronger than expected, while the blue, approaching peak is weaker. Both differences appear to dominate in the low-velocity portions of each component in the profile (presumably formed in gas close to a stellar photosphere where the wind acceleration is just beginning). The simplest explanation for this discrepancy is that the emitting gas distribution can also act to attenuate the stellar flux when the source clouds are seen in projection in front of the stellar disks.

Suppose that both stars have relatively larger outflows in the direction of their mutual companion, i.e., enhanced flow from Star 1 to Star 2 and from Star 2 to Star 1 in the region between the stars. In both cases, the outflow is seen with greatest projection against the source star when the outflow is in front of the star (leading to a decrease in line strength because of the partial absorption of the background stellar flux), and this produces blueshifted absorption (an incipient P Cygni-type absorption trough). On the other hand, this absorption vanishes when the outflow is behind the star and

directed away from us (projected against the sky), and then we observe the maximal redshifted emission. If the gas flow is mainly distributed near the axis joining the stars, then for the low orbital inclination of HD 149404, the gas flow is never seen fully in front or behind the source star, and we see only a minor variation in strength with extrema at the conjunctions (as observed).

We conclude that two flows must exist (to account for the two peaks in the tomograms) and that they are directed along and spatially coincident with the axis joining the stars (to account for their observed velocity patterns and phase-dependent attenuations, respectively). The only acceptable location is in outflows between the stars since the emission velocity distributions are inconsistent with the larger orbital motions that would be observed if the flows were placed on the outer facing hemispheres of both stars, for example. Thus, we suggest that the bulk of the emission originates in gas flows from both stars that are moving toward a colliding winds shock zone between the stars.

This simple model explains the V_X components of motion along the axis joining the stars, and the smaller V_Y components probably reflect the rapid rotation of the stars. Since both stars have supersynchronous rotation rates, we expect that gas flows leaving their surfaces would share this motion. Thus, the apparent motions of the gas flows (see the vectors placed between the stars in Fig. 6) represent the vector sum of radial outflow and rotational deflection.

The model we envision is sketched in Figure 6. The winds collide in the gap between the stars (shown as the shaded area). Note that the location and size of the shock region is given in a schematic illustration only, whereas the actual shock boundary is defined by the balance of wind momenta. The winds of the stars themselves may be concentrated toward the equatorial plane because of rapid rotation (Ignace, Cassinelli, & Bjorkman 1996) and/or focused toward the inner Lagrangian point by tidal effects (Friend & Castor 1982). The H α emission appears to be strongest in the material flowing into the shock region, and in fact, the emission strength probably drops significantly in the shock itself because the H α emissivity decreases with the higher temperatures found there (see Fig. 2 in Richards & Ratliff 1998). Once the gas cools as it moves out from the collision apex, it will once again emit more efficiently, and the broad

distribution of emission flux observed in the tomograms may result from emission over a large volume.

We can make an approximate estimate of the emission volume by calculating the total emission measure in H α . We used the stellar dimensions adopted above and stellar fluxes from Kurucz (1994) together with the average observed equivalent width of $W_\lambda = -5.3 \text{ \AA}$ to derive a total H α emission measure of $2.6 \times 10^{34} \text{ ergs s}^{-1}$. Then, using an emissivity coefficient for an assumed temperature of 36,000 K (Richards & Ratliff 1998) and a density of 10^{12} cm^{-3} (appropriate for the upper atmospheres of hot stars), we find an emitting volume of $2 \times 10^{35} \text{ cm}^3$, equivalent to a sphere of radius $5 R_\odot$. The gap between the stars is $\approx 18 R_\odot$ along the axis, and so the observed emission measure is consistent with an origin roughly between the stars if our temperature and density estimates are reasonable.

In summary, the tomograms of the H α emission profiles in HD 149404 suggest the presence of gas flows or focused winds that probably interact in a shock region. We find no evidence for present-day mass transfer in the system, which suggests that the evolution of the binary is being driven by stellar wind mass loss from the entire system. Future observations of HD 149404 (particularly high-resolution maps of the circumstellar gas surrounding the system) will help elucidate the nature of the colliding winds and the role this phenomenon plays in massive binary evolution.

We offer our thanks to the anonymous referee for criticisms that substantially improved this paper. We are deeply indebted to the Directors and Staff of MSO and ESO for their support of our observing runs. This research made use of the Simbad database, operated at Centre de Données astronomiques de Strasbourg, France. Institutional support was provided by the Georgia State University College of Arts and Sciences and the Research Program Enhancement fund of the Board of Regents of the University System of Georgia administered through the GSU office of the Vice President for Research and Sponsored Programs. This work was partially supported by NASA ADP grant NAG 5-2979 and the California Institute of Technology. Lex Kaper is supported by a fellowship of the Royal Academy of Sciences in the Netherlands. We gratefully acknowledge all of this support.

REFERENCES

- Bagnuolo, W. G., Jr., Gies, D. R., & Wiggs, M. S. 1992, *ApJ*, 385, 708
 Conti, P. S., Leep, E. M., & Lorre, J. J. 1977, *ApJ*, 214, 759
 Friend, D. B., & Castor, J. I. 1982, *ApJ*, 261, 293
 Gies, D. R., Bagnuolo, W. G. Jr., & Penny, L. R. 1997, *ApJ*, 479, 408
 Gies, D. R., & Wiggs, M. S. 1991, *ApJ*, 375, 321
 Gies, D. R., Wiggs, M. S., & Bagnuolo, W. G., Jr. 1993, *ApJ*, 403, 752
 Hutchings, J. B. 1976, *Publ. Dom. Astrophys. Obs. Victoria*, 14, 355
 Hutchings, J. B., & Van Heteren, J. 1981, *PASP*, 93, 626
 Ignace, R., Cassinelli, J. P., & Bjorkman, J. E. 1996, *ApJ*, 459, 671
 Jaschek, M., & Jaschek, C. 1974, *A&A*, 36, 401
 Jaschek, M., Jaschek, C., & Kuczewicz, B. 1964, *Z. Astrophys.*, 59, 108
 Kaithuck, R. H., Schlegel, E. M., Honeycutt, R. K., Horne, K. Marsh, T. R., White, J. C., II, & Mansperger, C. S. 1994, *ApJS*, 93, 519
 Kaper, L., Fullerton, A., Baade, D., de Jong, J., Henrichs, H., & Zaai, P. 1998, in *Cyclical Variability in Stellar Winds*, ed. L. Kaper & A. W. Fullerton (Berlin: Springer-Verlag), 103
 Kuczewicz, B. 1963, *PASP*, 75, 192
 Kurucz, R. L. 1994, Kurucz CD-ROM 19, Solar Abundance Model Atmospheres for 0, 1, 2, 4, 8 km/s (Cambridge: SAO)
 Lamers, H. J. G. L. M., & Leitherer, C. 1993, *ApJ*, 412, 771
 Maeder, A. 1999, *A&A*, 347, 185
 Mason, B. D., Gies, D. R., Hartkopf, W. I., Bagnuolo, W. G., Jr., ten Brummelaar, T., & McAlister, H. A. 1998, *AJ*, 115, 821
 Massey, P., & Conti, P. 1979, in *IAU Symp. 83, Mass Loss and Evolution of O-Type Stars*, ed. P. Conti & C. de Loore (Dordrecht: Reidel), 501
 Penny, L. R. 1996, Ph.D. thesis, Georgia State Univ.
 Penny, L. R., Gies, D. R., & Bagnuolo, W. G., Jr. 1999, in *IAU Symp. 193, Wolf-Rayet Phenomena in Massive Stars and Starburst Galaxies* ed. K. A. van der Hucht, G. Koenigsberger, & P. R. J. Eenens (San Francisco: ASP), 86
 Perryman, M. A. C. 1997, *The Hipparcos and Tycho Catalogues* (ESA SP-1200; Noordwijk: ESA/ESTEC)
 Puls, J., et al. 1996, *A&A*, 305, 171
 Richards, M. T., Jones, R. D., & Swain, M. A. 1996, *ApJ*, 459, 249
 Richards, M. T., & Ratliff, M. A. 1998, *ApJ*, 493, 326
 Schaller, G., Schaerer, D., Meynet, G., & Maeder, A. 1992, *A&AS*, 96, 269
 Stickland, D. J., & Koch, R. H. 1996, *Observatory*, 116, 145
 Thaller, M. L. 1997, *ApJ*, 487, 380
 Vanbeveren, D., & de Loore, C. 1980, *A&A*, 86, 21
 Vreux, J. M. 1985, *A&A*, 143, 209
 Wiggs, M. S., & Gies, D. R. 1992, *ApJ*, 396, 238
 ———. 1993, *ApJ*, 407, 252

Note added in proof.—G. Rauw et al. (*A&A*, in press [2001]) recently presented H α emission radial velocity results for HD 149404 that are similar to those reported here, but the authors prefer a different location for the colliding winds emission.